JOURNAL OF COORDINATION CHEMISTRY, 2018
https://doi.org/10.1080/00958972.2018.1442575

A soluble cyanide-bridged $\{Fe_4Ni_4\}$ box encapsulating a Cs^+ ion: synthesis, structure and electronic properties

Remi Plamont, Jessica Tami, Juan-Ramon Jimenez, Amina Benchohra, Omar Khaled, Geoffrey Gontard, Yanling Li and Rodrigue Lescouëzec

Institut Parisien de Chimie Moléculaire (IPCM), Sorbonne Université, CNRS, Paris, France

ABSTRACT

Cyanide coordination clusters have received attention for their electronic and magnetic properties. Here, we synthesized a new octametallic cyanide box encapsulating a Cs^+. The cationic complex $Cs\subset[Fe^{III}_4(Tp)_4Ni^{II}_4(^{NMe2}Tp)_4(\mu\text{-}CN)_{12}]^+$ was crystallized as a BF_4^- salt and its structure reveals that the cesium ion interacts with the twelve cyanide edges. These interactions are likely responsible for the remarkable stability of the supramolecular assembly, which maintains its integrity in solution, as shown by NMR spectroscopy, mass spectrometry, and cyclic voltammetry experiments. The ^1H NMR spectrum of **1** shows well-resolved signals, which are strongly shifted due to the paramagnetic nature of the cage. The encapsulated caesium ion is also affected by the paramagnetic cage and shows a strongly shifted ^{133}Cs paramagnetic NMR signal. The $\{Fe_4Ni_4\}$ box shows remarkable redox flexibility with five accessible oxidation states, which correspond to the reversible oxidation/reduction of the four Fe^{III}/Fe^{II} ions. The separation of the four consecutive redox waves accounts for the occurrence of an efficient electronic communication between the metal ions through the cyanide bridges. The cyanide bridges are also efficient in transmitting a ferromagnetic interaction between the iron and nickel ions as shown by the magnetic properties.

ARTICLE HISTORY
Received 10 December 2017
Accepted 18 January 2018

KEYWORDS
Molecular cage; cyanide ligand; electronic communication; caesium

CONTACT Rodrigue Lescouëzec rodrigue.lescouezec@upmc.fr, rodrigue.lescouezec@sorbonne-universite.fr
Supplemental data for this article can be accessed at https://doi.org/10.1080/00958972.2018.1442575

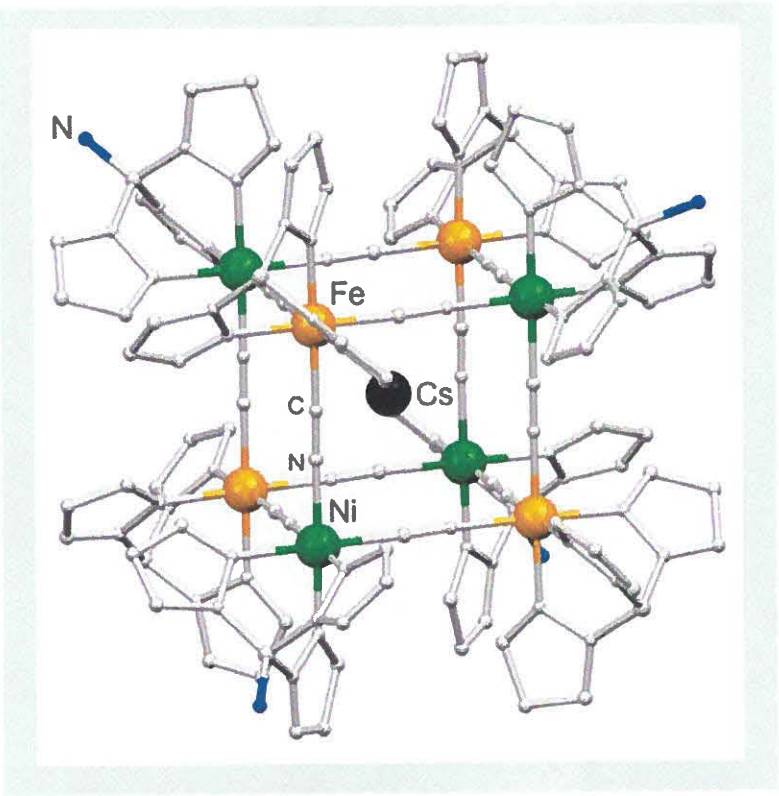

1. Introduction

Polymetallic cyanide assemblies have attracted interest because of their interesting electronic properties. These properties often arise from the ability of the cyanide ligand to promote efficient electronic communication between the metal ions it binds, through its set of σ and π frontier orbitals that are involved in the coordination bonds. The electronic communication is revealed, for example, in mixed valence compounds by the presence of a strong metal-metal charge transfer band, which can give an intense color. This is the case of Prussian blue, a mixed valence compound of class II (partially delocalized electron) of the formula $Fe^{III}_4[Fe^{II}(CN)_6]_3{\cdot}nH_2O$. This material is the first synthetic coordination polymer and was used as a blue pigment by painters during the eighteenth and nineteenth centuries [1]. Many Prussian blue analogs can be obtained by simply reacting hexacyanometallate with hexaaqua complexes. The resulting insoluble Prussian blue analogs (PBA) of general formula $A_xM'_4[M(CN)_6]_{(8+x)/3}[]_{(4-x)/3}{\cdot}nH_2O$ (A is an alkali cation, M and M′ are six-coordinate transition metal ions, [] represents a $[M(CN)_6]$ vacancy) are non-stoichiometric compounds, which all exhibit cubic structures where the octahedral metal ions are linked through linear cyanide bridges. Their electronic properties can be tuned by selecting the metal ion and by tuning the synthetic conditions to control the stoichiometry of the compound. The range of application for these emblematic cyanide-based coordination polymers is large and continuously broadening. For example, redox active PBA have been recently explored for water oxidation catalysis [2]. The electronic delocalization through the M–CN–M′ bridges and the possible insertion of alkali ions was used for PBA as cathode material in ion batteries [3]. When the metal ions bear unpaired electrons, the electronic communication gives magnetic exchange

interaction through the cyanide bridge (so-called superexchange interaction). Contrary to the oxo bridge, another efficient magnetic linker, the ambidentate character of the cyanide ligand and the use of stable cyanide building blocks, makes designing heterometallic compounds easier [4]. Moreover, the linear shape of the cyanide together with the rigidity of the $[M(CN)_6]^{x-}$ building block allows control on the topology of the final compounds. It is also possible to control the nature and the strength of the magnetic interaction using simple considerations. In particular, it has been shown that an adequate choice of the metal ions allows controlling the nature and the strength of the magnetic exchange interaction [5]. This allowed Verdaguer *et al.* to obtain the first molecular-based magnet with a Curie temperature above room temperature, VCr PBA [6]. The electronic communication through the cyanide bridge also allows, in some cases, the preparation of interesting mixed valence bistable systems, showing photo-induced electron transfer in the M–CN–M′ unit. The phenomenon was first observed by Sato in a FeCo Prussian blue analog [7] and it has been thoroughly investigated to better understand the phenomenon [8]. In the last two decades, more attention has been devoted to the synthesis of magnetic systems having reduced dimensionality. Besides curiosity-driven research, several reasons have motivated these works. Low-dimensional systems represent interesting models to help rationalize the magnetic properties of non-stoichiometric PBA. In contrast with PBA, they can also be soluble, although the stability of polymetallic species is rarely investigated. Low-dimensional systems can also show original physical properties. One possible synthetic strategy consists of using partially blocked cyanide building block $[M(L)(CN)_x]^{n-}$ (where L is an ancillary ligand) instead of hexacyanometallate during the self-assembly process. For example, we first showed that using the known $[Fe(L)(CN)_4]^-$ complex toward cobalt aqua-complexes (L = 2,2′-bipyridine or 1,10-phenanthroline), we could obtain magnetic 1-D chain compounds [9]. We later designed new pyrazolylborate-based $[Fe(^{R}Tp)(CN)_3]^-$ cyanide building block (Tp is a tris-(pyrazolyl)borate anion), which shows reduced coordination ability with only three cyanide ligands oriented in facial geometry [10]. These precursors led to many low-dimensional compounds showing interesting properties [11]. Although the intrinsic anisotropy of the magnetic properties of the building block is not underlined in these works, these precursors were proven successful to design slow relaxation systems [12]. In fact, from a magnetic point of view, these Fe^{III} low-spin complexes are remarkably anisotropic because of the first-order spin-orbit coupling contribution in the d^5 low-spin configuration [13]. The versatility of the pyrazolyl ligand, which allows adjusting the electronic properties of the complexes, was also useful in designing FeCo switchable compounds [12, 14] and multifunctional systems [15]. The search for new kinds of cyanide-based coordination assemblies is also interesting from a pure fundamental reason, and it has motivated us to look for new synthetic approaches. Using oxo-bridged polymetallic reactants toward the $[Fe(Tp)(CN)_3]^-$ building block, we obtained the largest cyanide-based coordination cluster containing 60 Fe metal ions [16]. More recently, our interest has been devoted to the design of molecular models of PBA. In particular, we have focused our attention on the synthesis of cyanide-bridged octametallic cages $A\subset\{Fe_4Co_4\}$ containing an inserted alkali ion, A [17]. These boxes are obtained by reacting the *fac*-$[Fe(Tp)(CN)_3]^-$ building block with *fac*-$[Co(^{Pz}Tp)(H_2O)_3]^{2+}$ in the presence of a templating alkali cation. They represent interesting molecular models which allow in depth study of the influence of the alkali ion on the electronic properties of the box, particularly on the photomagnetic effect. One of their specificities is to show remarkable stability in organic solvent, even under boiling conditions. In this context, we started exploring if

these cages could be obtained with other metal ions and with other blocking ligand. In this article, we report a new $\{Fe_4Ni_4\}$ neutral cage containing an encapsulated Cs^+ ion. The ^{R}Tp ligand we used here is a new heteroscorpionate [19], with the R group being $N(Me)_2$. We thus describe in this work the synthesis of the new ligand, the $Cs\subset\{Fe_4Ni_4\}$ cage, its structure, and its solution and solid-state studies, which allowed us to probe the electronic properties of the cage and its stability in solution.

2. Experimental

2.1. General methods

FT-IR spectra were collected in the 200–4000 cm^{-1} range. Measurements were carried out on a Vertex 70 Brüker instrument using the attenuated total reflection (ATR) technique on solid samples (with a 4 cm^{-1} resolution). The intensity of the absorption band is indicated as w (weak), m (medium), s (strong), vs (very strong), and br (broad).

NMR spectra were recorded on a Bruker Avance 400 spectrometer. The chemical shifts, δ, are expressed in parts per million (ppm) and are referenced using IUPAC recommendations. All the measurements of the paramagnetic sample were carried out after thermal stabilization.

Mass spectrometric analyses (ESI mode MS mode) were performed on a micro-TOF Bruker mass spectrometer. The Cs-cube was measured in dichloromethane by direct infusion with the ESI-source set at 180 °C and a capillary voltage set at 4500 V.

Elemental analyses (C, H, and N) were carried out by combustion analysis using a vario MICRO cube apparatus from Elementar.

DC and AC Magnetic susceptibility measurements were carried out using, respectively, a Quantum Design MPMS-XL7 magnetometer and a PPMS-9 susceptometer. The DC measurements were performed from 2 to 300 K under a 0.2 T magnetic field. A lower field of 0.05 T was also used in the low temperature range (2–40 K) to avoid saturation effect. A fresh sample of the Cs-cube was filtered from the mother solution and wrapped in a PVC film just before its introduction into the MPMS at 120 K under helium flow. It was frozen in the magnetometer before purging under vacuum to prevent the evaporation of the crystallized solvent molecules. The DC magnetic susceptibility values were corrected from the diamagnetism of the molecular constituents and of the sample holder. The AC measurements were carried out on a sample prepared in the same manner as that described above. The measurements were taken at 3 K with different static magnetic fields, from 0 to 4999 Oe. The AC amplitude was set to 10 Oe and the frequency range varied from 10 to 9900 Hz. No ac susceptibility signals were observed.

Cyclic voltammetry measurements were carried out at room temperature in a standard cell equipped with a platinum wire counter electrode, a calomel reference electrode (ECS) and a glassy-carbon working electrode using an AUTOLAB PGSTAT 100 electrochemical analyser. The measurements were performed in dichloromethane with 0.1 M $[Bu_4N][PF_6]$ as the supporting electrolyte at scan rates of 100 mV s^{-1}. The redox potentials were determined by using ferrocene/ferrocenium couple (Fc/Fc^+) as an internal reference.

2.2. Syntheses

2.2.1. Synthesis of ^{NMe2}Tp dimethylamino-tris(pyrazolyl)borate

In a three-necked round bottom flask, sodium pyrazolate, NaPz (0.7 g, 7.7 mmol) and pyrazolyl, HPz (1.04 g, 15 mmol) were dissolved under argon in 10 mL of dried THF. To this solution, 1.35 mL of tris(dimethylamino)borane, $B(N(Me)_2)_3$ (7.7 mmol) and 10 mL of toluene were added. The reaction mixture was refluxed for 24 h. After cooling the reaction mixture to room temperature, a white precipitate was collected by filtration and washed with 10 mL of dried hexane, affording 1.4 g of white powder. The compound was stored in argon. Yield: 65%. ^{1}H NMR (400 MHz, CD_3CN) δ : 7.54 (d, 3H, Pz-H), 7.47 (d, 3H, Pz-H), 6.10 (dd, 3H, Pz-H), 2.16 ppm (s, 6H, $N(CH_3)_2$). ^{11}B NMR (133 MHz, CD_3CN): δ: 2.61 ppm.

2.2.2. Synthesis of $Cs\subset[Fe^{III}_4(Tp)_4Ni^{II}_4(^{NMe2}Tp)_4(CN)_{12}]\cdot BF_4.2C_6H_{14}.CH_2Cl_2$ (1)

The starting material, tris(pyrazolyl)borate (KTp), was obtained as described by Trofimenko [19]. The complex $NBu_4[Fe^{III}(Tp)(CN)_3]$ was obtained as described by Lescouëzec *et al.*, replacing the PPH_4^+ counterion by the NBu_4^+ [10]. All other chemicals were obtained as reagent grade from usual commercial sources and used without purification. To prepare the iron-nickel cube, we separately dissolved 0.2 mmol (0.118 g) of $NBu_4[Fe^{III}(Tp)(CN)_3]$ in 2 mL DMF, 0.2 mmol (0.068 g) of $Ni(BF_4)_2{\cdot}6H_2O$ in 2 mL DMF, 0.8 mmol (0.186 g) of $CsClO_4$ in 3 mL of DMF, and 0.4 mmol (0.120 g) of $Na^{NMe2}Tp$ in 2 mL of DMF. Each component was added dropwise to the beaker containing the iron solution in respective order while stirring. The solution immediately turned orange-red with the addition of nickel to iron, and turned even darker with the cesium salt; the ligand had no effect on the color of the solution. The solution stirred for 15 min and was filtered to remove the excess of $CsClO_4$ precipitate. An excess of diethyl ether was added to precipitate the cube. For purification, the precipitate was then dissolved in acetonitrile, precipitated again with an excess of ether, and filtered. The collected solid was dissolved a final time in a minimal amount of dichloromethane, filtered, and transplanted to the bottom of hexane in a test tube via syringe for crystallization. The test tube was covered with parafilm and was left untouched until crystals formed. Yield: 60%. ^{1}H NMR and ^{133}Cs NMR (400 MHz, CD_2Cl_2) are detailed below. FT-IR spectrum (KBr): $\nu_{(CN)}$ stretching: 2160 cm^{-1}; $\nu_{(BH)}$: 2510 cm^{-1}. Characteristic bands of the ^{R}Tp ligands: 2123(w) (CH_3 of ^{NMe}Tp), 1506(m), 1407(s), 1313(s), 1213(s), 759(s). Characteristic bands of BF_4^-: 1120, 1049 cm^{-1}. Anal. Calcd for $C_{105}H_{129}B_9Cl_2CsF_4Fe_4N_{64}Ni_4$: C, 40.29; H, 4.15; N, 28.64. Found: C, 40.48; H, 3.89; N, 28.98. MW: 3129.7 g/mol.

2.3. X-ray crystallography

Red prismatic crystals of **1** suitable for X-ray diffraction studies were grown by diffusion of hexane into a solution of **1** in dichloromethane at room temperature. A single crystal was selected, mounted, and transferred into a cold nitrogen gas stream. Intensity data were collected with a Bruker Kappa-APEX2 system using fine-focus sealed tube Mo-Kα radiation (Table 1). Unit-cell parameter determination, data collection strategy, integration and absorption correction were carried out with the Bruker APEX2 suite of programs. The structure was solved with SHELXT-2014 and refined anisotropically by full-matrix least-squares methods with SHELXL-2014 using the WinGX suite. The structure contains a lot of disorder. The counter-anion to the cesium ion is missing. Other analyses identified it as being a

Table 1. Crystallographic data and structure refinement for 1.

Empirical formula	$C_{101}H_{117}B_8CsFe_4N_{67}Ni_4O_3$
Formula weight	
Temperature	130(1) K
Wavelength	0.71073 Å
Crystal system	Trigonal
Space group	R –3
Unit cell dimensions	a = b = 20.4574(15) Å, c = 39.943(3) Å, $\alpha = \beta = 90°$, $\gamma = 120°$
Volume	$V = 14477(2)$ Å^3
Z	3
Absorption coefficient	0.910 mm^{-1}
Min/max transmission	0.64/0.86
Theta range for data collection	1.26°–26.54°
Reflections collected	57632
Independent reflections	6634 ($R_{int} = 0.051$)
Observed reflections [I > 2σ(I)]	6634
Completeness	0.988
Restraints/parameters	140/354
[a]Final R indices [I > 2σ(I)]	$R_1 = 0.1228$, $wR_2 = 0.4259$ (all data)
[b]Goodness-of-fit on F^2	1.606
Largest diff. peak and hole	5.16/–0.92 e.Å^{-3}

[a]$R_1 = \Sigma(|Fo| - |Fc|)/\Sigma|Fo|$; $wR_2 = [\Sigma w(Fo^2 - Fc^2)^2/\Sigma w(Fo^2)^2]^{1/2}$.
[b]$S = [\Sigma w(|Fo| - |Fc|)^2/(No - Np)]^{1/2}$.

tetrafluoroborate but it could not be located on the Fourier difference map. It is believed to be somewhere between the cube and the channels of disordered solvent (vide infra) but disordered onto many positions. The cubes are statistically disordered with iron and nickel ions roughly occupying the same positions within the structure. Several atoms of the trispyrazolylborate ligands are located on average positions between two or more possible conformations. As a result, some of these atoms seem to be much too close to one another, most notably C3 to C11A, C3 to C11B, C16 to C17, and C16 to C18. The cesium is not effectively located at the center of the cube, which explains the remaining electron density calculated on its position. The structure also contains very large channels of severely disordered and partially evaporated molecules of dimethylformamide and/or diethylether, which could not be properly located. PLATON-SQUEEZE was instead used for the final refinement cycle to further refine the structure while accounting for the corresponding unassigned electron density. The structure was deposited at the Cambridge Crystallographic Data Center with number CCDC 1588704 and can be obtained free of charge via www.ccdc.cam.ac.uk.

3. Results and discussion

3.1. Structure

Despite our efforts, the crystallographic data obtained on single crystals of **1** are of limited quality. However, they allow the confirmation of other analytical data obtained by mass spectrometry, elemental analysis, FT-IR, NMR, and magnetism (see below). Compound **1**, of the formula $Cs\subset[Fe^{III}_4(Tp)_4Ni^{II}_4(^{NMe2}Tp)_4(CN)_{12}]\cdot BF_4\cdot 2C_6H_{14}\cdot CH_2Cl_2$, crystallizes in the $P2_1/n$ monoclinic space group. The octametallic complex exhibits a cubic core made of M–CN–M′ edges and trispyrazolyl-borate ancillary ligands occupying the eight corners (Figure 1). A cesium ion occupies the center of the $\{Fe_4Ni_4\}$ box. Compound **1** is thus similar to the

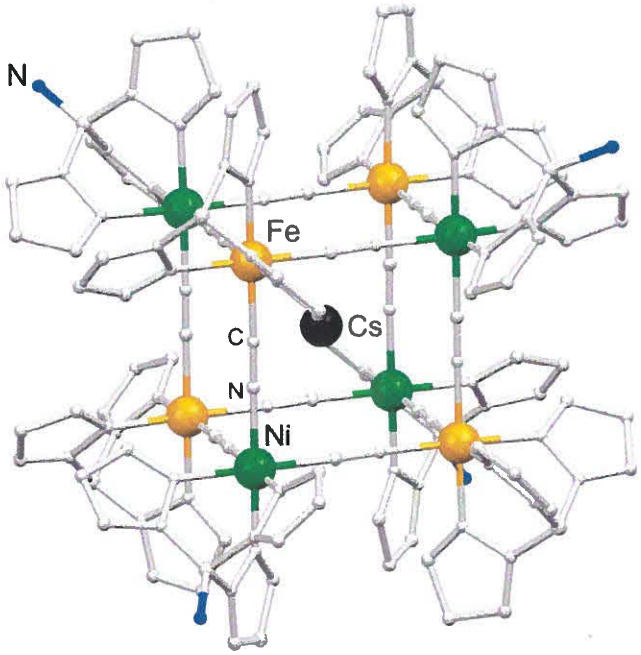

Figure 1. View of the X-ray structure of Cs-cube (recorded at 200 K). (C and N of the skeleton: gray; N (NMe_2): blue; Ni: green; Fe: yellow; Cs: black). Lattice solvents, hydrogens and disordered methyl groups of the $N(Me)_2$ groups are omitted for clarity.

$Cs\subset\{Fe^{II}_4Co^{III}_3Co^{II}\}$ cube that was recently reported [17]. The asymmetric unit is made of a cube edge, where one metal has an occupancy of 1 and the other 1/3. The Fe and Ni metal ions, and the Tp and ^{NMe2}Tp ancillary ligands are indiscernible. Thus, the bond distances and angles are averaged values and cannot be analyzed in detail. However, the Fe–CN–Ni bond length, *ca.* 5.11 Å, is as expected for a Fe^{III}–CN–Ni^{II} bridge [20]. The cubic molecules are quite well isolated from each other by the organic shell formed by the ligand and the shortest intermolecular M···M distance is *ca.* 11.6 Å.

3.2. ^{1}H and ^{133}Cs NMR

The ^{1}H NMR spectrum of **1** was recorded in CD_2Cl_2. It shows various strongly shifted signals that account for the paramagnetic nature of the molecule (Figure 2). At 300 K, the ^{1}H signals spread in a large chemical shift range, from *ca.*+58 to −55 ppm. Despite the presence of eight paramagnetic centers in the molecules, the peak half-widths remain moderate so that reliable peak integration can be obtained. Beside the residual solvent peaks, eight paramagnetic signals are expected when taking into account the cubic symmetry of the molecule: (i) 6 different proton signals integrating for 12 H each are assigned to the pyrazolyl protons of the two scorpionate ligands; (ii) one proton signal integrating for 4 H due to the BH groups of the four equivalent Tp ligands; (iii) one signal integrating for 24 H, assigned to the methyl groups of the four equivalent ^{NMe2}Tp ligands. The peak intensity allows the unambiguous assignment of the BH at +40.0 ppm and the methyl groups at +1.5 ppm. The peak of the Tp ligand can be identified by comparing the ^{1}H spectrum of **1** to that of $PPh_4[Fe^{III}(Tp)(CN)_3]$ [21] or $NBu_4[Fe^{III}(Tp)(CN)_3]$ precursors obtained in the same solvent at the same temperature

(see Figure S1). As the BH signal is very similar in both cases (+40 ppm in **1** and +42 ppm in the precursor), we assumed that the ^{1}H pyrazolyl signals were not significantly affected by the coordination to the Ni(II). In fact, three proton signals very similar to those of the $PPh_4[Fe^{III}(Tp)(CN)_3]$ precursor are found at −12.8, −15.7 and −54.7 ppm. The broadest signal at −54.7 can be assigned to the proton Ha, which is located close to the metal ion (Fe···Ha < 4 Å). In fact, the proton signals located close to the metal paramagnetic source are broadened because of the larger contribution of the electron-nuclei dipolar interaction. This interaction led to a faster magnetic relaxation and a broadening of the NMR signals [22]. The other two signals, Hb (−15.7 ppm) and Hc (−12.8 ppm) were assigned by comparison with those found in the $PPh_4[Fe(Tp)(CN)_3]$ precursor. The three remaining strongly shifted signals integrating for 12H each, were thus assigned to the three pyrazolyl protons of the four equivalent ^{NMe2}Tp ligands coordinated to Ni(II). Because of the larger half-width of the signal located at +32.8 ppm, it is reasonable to assign this signal to the proton located close to the Ni paramagnetic source, Ha'. The other two signals at +57.8 and +49.4 ppm are assigned to Hb' and Hc'. Finally, it is worth noticing that the ^{1}H NMR of **1** does not show any other paramagnetic or diamagnetic signals (expect those of the residual solvent molecules). This accounts for the purity of the sample and the robustness of the cubic cage in organic solvent.

The ^{133}Cs spectrum of **1** was also recorded at 300 K in CD_2Cl_2 (Figure 2, inset). Although ^{133}Cs has a quadrupolar nucleus, its quadrupole moment is very weak and its receptivity is good so that well-resolved narrow signal can be obtained in solution [23]. In the present case, only one ^{133}Cs signal is observed, which is consistent with the presence of only one cesium site in a cubic surrounding. The ^{133}Cs signal is remarkably shifted upfield at −780 ppm, far away from the diamagnetic range (*vs.* $CsNO_3$ in D_2O). This accounts for efficient electronic

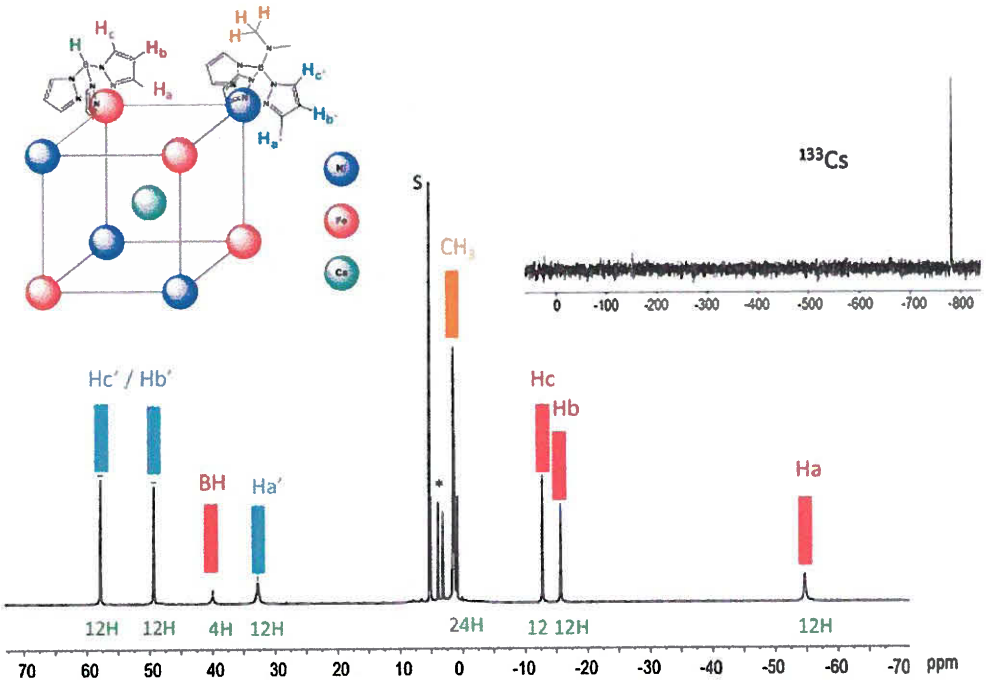

Figure 2. ^{1}H NMR spectrum of 1 in CD_2Cl_2 at 300 K together with the signal assignment (the peak integration is given below the peaks). Inset (right): ^{133}Cs NMR of 1 at 300 K in CD_2Cl_2.

communication between the paramagnetic sources and the inserted alkali ion. The observed chemical shift can be compared with two reference compounds. The measured value (–780 ppm) is smaller than that observed in the 3-D $CsNi^{II}[Co^{III}(CN)_6]$ Prussian blue analog (–946 ppm at 298 K) [24], where each cesium ion is located inside a cubic cage formed by four paramagnetic Ni(II) ions and four diamagnetic Co(III) ions, and it is larger than that observed in the $Cs\subset\{Fe^{II}_4Co^{III}_3Co^{II}\}$ molecular cage (–236 ppm at 300 K) [16] where only one paramagnetic high-spin Co^{II} ion is present. The observed paramagnetic chemical shift consists of two contributions, $\delta^{para} = \delta^{dip} + \delta^{con}$: (i) δ^{dip} is the dipolar contribution due to the through space electron-nucleus dipolar magnetic interaction; (ii) δ^{con} is a contact term due to the spin delocalization onto the observed nucleus. As mentioned in the two reference works, the dipolar contribution is expected to be positive or negligible. The negative experimental chemical shift can thus only be explained by a negative contact contribution. This implies some spin transfer from the paramagnetic sources to the central Cs atom, either directly from the metal frontier orbitals to the cesium [24], or indirectly through the interaction of the Cs^+ ion with the CN ligands [17].

3.3. Cyclic voltammetry

The cyclic voltammogram of **1** (Figure 3) has been recorded in CH_2Cl_2 (see details in the Experimental section). It shows four quasi-reversible redox waves corresponding to the successive reduction of the Fe^{III} ions: $[Fe^{III}_4Ni^{II}_4]/[Fe^{III}_3Fe^{II}Ni_4]^-$, $E°_{1/2} = -0.36$ V; $[Fe^{III}_3Fe^{II}Ni^{II}_4]^-/[Fe^{III}_2Fe^{II}_2Ni^{II}_4]^{2-}$, $E°_{1/2} = -0.47$ V; $[Fe^{III}_2Fe^{II}_2Ni^{II}_4]^{2-}/[Fe^{III}Fe^{II}_3Ni^{II}_4]^{3-}$, $E°_{1/2} = -0.65$ V; $[Fe^{III}Fe^{II}_3Ni^{II}_4]^{3-}/[Fe^{II}_4Ni^{II}_4]^{4-}$, $E°_{1/2} = -0.86$ V (*vs* ferrocene, Fc). As expected, the first redox potential at –0.36 V is significantly higher compared to that of the precursor $[Fe^{III}(Tp)(CN)_3]^-$ ($E°_{1/2} = -0.89$ V, *vs* Fc) [25]. This is consistent with coordination of Lewis acids (the Ni(II) ions) on the nitrogen of the cyanide ligands. The donation from the nitrogen to the Ni(II) reduces the electronic density of the whole $\{Fe(Tp)(CN)_3\}$ subunit and makes the $Fe^{II/III}$ oxidation more difficult. The effect decreases on the second, third and fourth reduction waves as the cage becomes more and more negatively charged. In fact, the last reduction wave is found at about the same potential as that of the free $[Fe(Tp)(CN)_3]^-$ complex. It is interesting to compare this effect

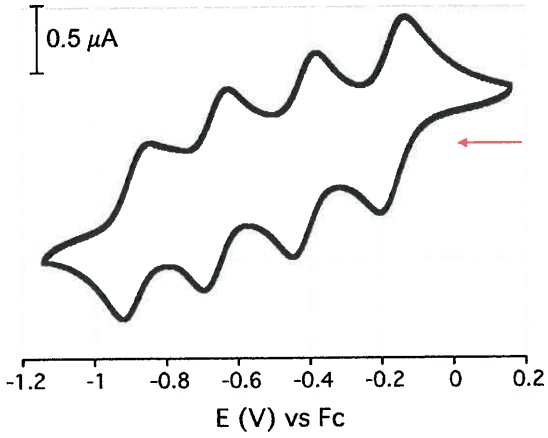

Figure 3. Cyclic voltammogram of 1 in CH_2Cl_2 (*vs* Fc; WE: C; CE: Pt wire; 0.1 V/s).

with that observed in related $\{Fe_4M_4\}$ cages containing similar ancillary scorpionate ligands with other metal ions coordinated on the nitrogen of cyanide. The shift of the $\{Fe^{II/III}(Tp)(CN)_3\}$ redox potential to higher values is much more important in the $\{Fe^{III}{}_4Fe^{II}{}_4\}$ cages reported by Oshio *et al.* [26]. In that case, the nitrogen is coordinated to the very acidic Fe^{III} ions and the redox waves are located approximately 1.4 V above those found in our $\{Fe_4Ni_4\}$ cage. The effect is similar in our recently reported $Cs\subset\{Fe_4Co_4\}$ cage [17]. The redox potentials are shifted by *ca.* 1.15 V in comparison to **1**. In these last cases, the potential of the $\{Fe^{II/III}(Tp)(CN)_3\}$ units in the cage become high compared to that of the coordinated neighbor (initially Fe^{II} and Co^{II} ion) and an electron transfer occurs during the synthesis between the neighboring metal ions.

It is also interesting to compare the differences between the four successive Fe^{II}/Fe^{III} redox waves in these cubes. These shifts account for an efficient electronic communication between the four iron ions in the $\{Fe_4Ni_4\}$ cage. The interaction can be quantified by the comproportionation constants, K_c, which reflects the relative stability of the mixed valence states with respect to its (monovalent) reduced and oxidation forms. The comproportionation constant is calculated through the expression $K_c = \exp(F\Delta E/RT)$, where ΔE is the difference between successive oxidation waves. $|\Delta E|$ values of 0.23, 0.25 and 0.24 V for the four redox waves yield to K_c of 7.3×10^3, 1.5×10^4 and 1.0×10^4. These values are in the expected range for mixed-valence Class II compounds [27]. Here, this interaction takes place between second neighbors through the –CN–Ni–NC– bridge. The obtained values are about 10 times bigger than those

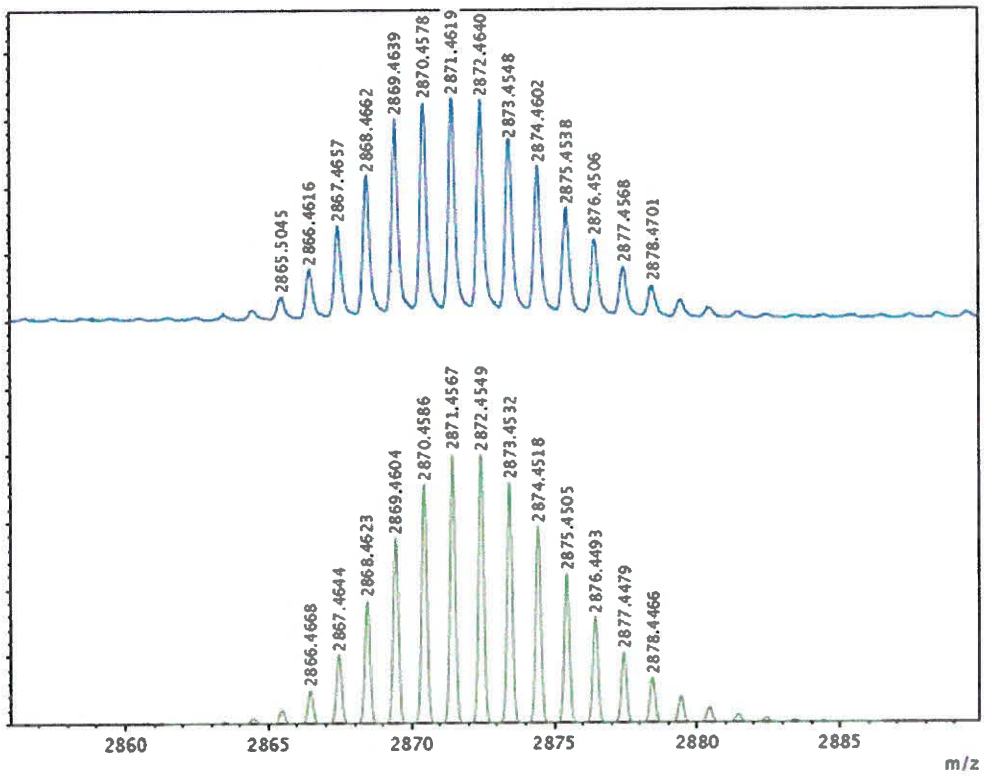

Figure 4. Experimental (top) and simulated (bottom) mass spectrum of 1.

found in the above-mentioned $\{Fe_4Fe_4\}$ [26], $\{Fe_4Co_4\}$ [17] molecular cubes, thus suggesting a larger communication between the iron ions in **1**.

It is worth underlining here that both NMR and electrochemistry studies account for the stability of the cube in solution. These results are also consistent with the mass spectrometry experiment, which shows a molecular peak corresponding to $\{\mathbf{Li,1}\}^+$ at 2871.45 g/mol. The simulated isotopic distribution is perfectly coherent with the experimental one as shown in Figure 4.

3.4. Magnetic properties

The magnetic properties of a polycrystalline sample of **1** have been investigated from 2 to 300 K. The $\chi_M T$ versus T plot of **1** is shown in Figure 5 (χ_M being the molar magnetic susceptibility per $\{Fe^{III}_4Ni^{II}_4\}$ unit). The value of the $\chi_M T$ product at room temperature (7.9 $cm^3\,K\,mol^{-1}$) is in agreement with the expected value considering the following set of uncoupled spin carriers: four low-spin iron(III) ions exhibiting magnetic orbital contribution (*ca.* $\chi_M T \approx 0.5$–$0.8\ cm^3\,K\,mol^{-1}$, with $g_{av} \approx 2.6$) and four nickel(II) ions (*ca.* $\chi_M T \approx 1.1\ cm^3\,K\,mol^{-1}$ with $g \approx 2.1$) [10, 28]. Upon cooling, the $\chi_M T$ value decreases smoothly to *ca.* 125 K, where $\chi_M T$ reaches $7.3\ cm^3\,K\,mol^{-1}$. This smooth decrease is ascribed to the spin-orbit coupling effect of the four Fe^{III} low-spin ions. Below 125 K, the $\chi_M T$ value increases rapidly, reaching a maximum at 5 K of $16.5\ cm^3\,K\,mol^{-1}$. Then a slight decrease is observed due to the combined effects of the magnetic ground state anisotropy and the intermolecular interaction. The strong increase is in agreement with an intramolecular ferromagnetic interaction. This is as expected for a Fe–CN–Ni moieties where the magnetic orbitals on both metal ions (t_{2g} and e_g, respectively) are orthogonal [29] as previously observed in other cyanide-bridged FeNi complexes [28]. The isothermal magnetization of **1** versus magnetic field (Figure S2) shows that the magnetic moment tends to saturate with increasing of the magnetic field and reaches the value of 11.8 μ_B at 7 T, indicating a ground spin state of $S = 6$ for **1**, which is in agreement with a ferromagnetic interaction. In order to evaluate the overall coupling constant of the ferromagnetic interactions through the cyanide bridge, the following spin Hamiltonian (Equation 1) has been used to fit the experimental $\chi_M T$ data in the temperature range of 30–300 K using free Phi software [30],

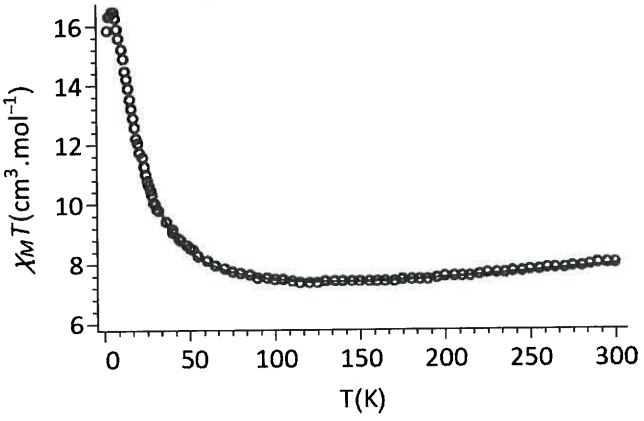

Figure 5. Plot of the $\chi_M T$ *vs* T product in the 2–300 K temperature range in 1. Solid line represents the Phi simulation of the data above 30 K.

$$H = -2J_{iso}\left[S_{Ni1}\left(S_{Fe2} + S_{Fe3} + S_{Fe4}\right) + S_{Ni2}\left(S_{Fe1} + S_{Fe3} + S_{Fe4}\right) + S_{Ni3}\left(S_{Fe1} + S_{Fe2} + S_{Fe4}\right) + S_{Ni4}\left(S_{Fe1} + S_{Fe2} + S_{Fe3}\right)\right] + g_{Ni}\left(S_{Ni1} + S_{Ni2} + S_{Ni3} + S_{Ni4}\right)H\beta + g_{Fe}\left(S_{Fe1} + S_{Fe2} + S_{Fe3} + S_{Fe4}\right)H\beta \quad (1)$$

where J_{iso} is the isotropic coupling constant between the low-spin Fe^{III} and the Ni^{II} ions, S_{Fek} is the spin operator for low spin Fe^{III} ($S_{Fek} = ½$, $k = 1$–4) and S_{Nik}, the spin operator for Ni^{II} ($S_{Nik} = 1$, $k = 1$–4), g_{Ni} and g_{Fe} are the Landé factors of the Ni^{II} and Fe^{III} ions, respectively, β is the Bohr magneton, and H is the applied magnetic field. The best fit gives: $J_{iso} = 4.95\ cm^{-1}$, $g_{Ni} = 2.0$ and $g_{Fe} = 2.2$. The two later values are obviously too low compared to the expected g_{Ni} and g_{Fe} values (see above). However, although the simplified spin Hamiltonian under-estimates the Landé factors of the metal ions, it allows a fair estimation of the average ferromagnetic coupling constant, J_{iso}. Here, the J_{iso} value obtained is reasonable and is of the same magnitude as that reported for Fe^{III}–Ni^{II} ferromagnetic couplings through a cyanide linker [20, 31]. Finally ac susceptibility measurements were carried out at low temperature to probe the occurrence of slow magnetic relaxation in the $S = 6$ ground spin-state. Although both low-spin Fe^{III} and Ni^{II} show magnetic anisotropy in distorted octahedral geometry, no out-of-phase signal was detected (at zero magnetic field and under the application of small dc field). The absence of slow magnetic relaxation in **1** is consistent with the high symmetry of the octametallic complex.

4. Conclusion

We showed that the synthetic approach that we recently used to prepare FeCo switchable cubic cages containing tris(pyrazolyl)borate ancillary ligands and an inserted alkali ion can be extended to the use of other metal ions or other functionalized scorpionate ligands. The new $Cs\subset\{Fe_4Ni_4\}$ cationic cage can be obtained as single crystals in good yield. As for the parent $Cs\subset\{Fe_4Co_4\}$ cube, it is soluble and stable in organic solvent as demonstrated by the NMR and electrochemistry studies. The cyclic-voltammetry study also shows the remarkable redox flexibility of the $Cs\subset\{Fe_4Ni_4\}$ cage, which shows five accessible redox states. Moreover, the ^{133}Cs NMR spectrum shows that a noticeable amount of spin density is transferred from the paramagnetic centers to the inserted cesium ion. This brings experimental proof of the occurrence of a through-bond electronic interaction between the inserted cesium and the paramagnetic box. This study also reveals an efficient electronic interaction between the second neighbor iron ions. Additionally, the electronic interaction trough the cyanide bridge between the first neighbor is revealed by the occurrence of a ferromagnetic superexchange interaction between the Fe(III) and Ni(II) ions, which leads to a $S = 6$ ground spin state. The absence of slow magnetic relaxation despite the presence of anisotropic paramagnetic ions is likely due to the high symmetry of the molecule. Our synthetic efforts are now focusing on the design of new stable cubes with peripheral anchoring groups in order to insert these functional polymetallic units into more sophisticated hybrid materials.

Supplementary materials

The structure was deposited at the Cambridge Crystallographic Data Center with number CCDC 1588704. Copy of this information may be obtained free of charge on application to CCDC, 12 Union

Road, Cambridge CB2 1EZ, UK (Fax:+44 1223 336 033; E-mail: deposit@ccdc.cam.ac.uk or www: http://www.ccdc.cam.ac.uk). Supplementary data associated with this article: ^{1}H NMR spectra of $NBu_4[Fe(Tp)(CN)_3]$ in CD_2Cl_2 at 300 K (Figure S1); curve of the magnetization versus applied magnetic field (H) for **1** at 2 K (Figure S2).

Acknowledgements

We are grateful to the CNRS, le ministère de l'enseignement et de la recherche and the Agence Nationale de la Recherche (ANR-JST program, MoMa project, ANR-14-JTIC-0001), and the National Science Foundation (CHE-1659782).

Disclosure statement

No potential conflict of interest was reported by the authors.

Funding

This work was supported by the Agence Nationale de la Recherche (ANR-JST program, MoMa project, [grant number ANR-14-JTIC-0001]), and the National Science Foundation [grant number CHE-1659782].

ORCID

Rodrigue Lescouëzec http://orcid.org/0000-0003-3510-5112

References

[1] (a) J. Woodward. *Philos. Trans.*, **33**, 15 (1724); (b) F. Grandjean, L. Samain, G.J. Long. *Dalton Trans.*, **45**, 18018 (2016).
[2] (a) S. Pintado, S. Goberna-Ferrón, E. Escudero-Adán, J.R. Galán-Mascarós. *J. Am. Chem. Soc.*, **135**, 13270 (2013); (b) S. Goberna-Ferrón, W. Hernández, B. Rodríguez-García, J.R. Galán-Mascarós. *ACS Catal.*, **4**, 1637 (2014); (c) J.R. Galán-Mascarós. *ChemElectroChem*, **2**, 37 (2015).
[3] (a) M. Okubo, D. Asakura, Y. Mizuno, J.D. Kim, T. Mizokawa, T. Kudo, I. Honma. *J. Phy. Chem. Lett.*, **1**, 2063 (2010); (b) Y. Lu, L. Wang, J. Cheng, J.B. Goodenough. *Chem. Commun.*, **48**, 6544 (2012); (c) C.D. Wessells, S.V. Peddada, R.A. Huggins, Y. Cui. *Nano Lett.*, **11**, 5421 (2011); (d) C.D. Wessells, R.A. Huggins, Y. Cui. *Nat. Commun.*, **2**, 550 (2011); (e) A.L. Lipson, S.D. Han, S. Kim, B.F. Pan, N.Y. Sa, C. Liao, T.T. Fister, A.K. Burrell, J.T. Vaughey, B.J. Ingram. *J. Power Sources*, **325**, 646 (2016); (f) Z. Li, K. Xiang, W.T. Xing, W.C. Carter, Y.M. Chiang. *Adv. Energy Mater.*, **5**, 1401410 (2015).
[4] M. Shatruk, C. Avendano, K.R. Dunbar. *Prog. Inorg Chem.*, **56**, 155 (2009).
[5] M. Verdaguer, A. Bleuzen, C. Train, R. Garde, F. Fabrizi, C. Desplanches. *Phil. Trans. A.*, **357**, 1762 (1999).
[6] (a) S. Ferlay, T. Mallah, R. Ouahès, P. Veillet, M. Verdaguer. *Nature*, **378**, 701 (1995); (b) S.M. Holmes, G.S. Girolami. *J. Am. Chem. Soc.*, **121**, 5593 (1999).
[7] O. Sato, T. Iyoda, A. Fujishima, K. Hashimoto. *Science*, **272**, 704 (1996).
[8] A. Bleuzen, V. Escax, A. Ferrier, F. Villain, M. Verdaguer, P. Münsch, J-P. Itié. *Angew. Chem. Int. Ed.*, **116**, 3814 (2004).
[9] (a) R. Lescouëzec, F. Lloret, M. Julve, J. Vaissermann, C. Ruiz-Pérez, M. Verdaguer, W. Wernsdorfer, D. Gatteschi. *Angew. Chem. Int. Ed.*, **13**, 1483 (2003); (b) L. Toma, R. Lescouëzec, F. Lloret, M. Julve, J. Vaissermann, M. Verdaguer. *Chem. Commun.*, **15**, 1850 (2003); (c) R. Lescouëzec, L. Toma, J. Vaissermann, M. Verdaguer, F.S. Delgado, C. Ruiz Perez, F. Lloret, M. Julve. *Coord. Chem. Rev.*, **249**, 2691 (2005); (d) L.M. Toma, R. Lescouëzec, J. Pasán, C. Ruiz Pérez, J. Vaissermann, J. Cano, R. Carrasco, W. Wernsdorfer, F. Lloret, M. Julve. *J. Am. Chem. Soc.*, **128**, 4842 (2006).

[10] (a) R. Lescouëzec. PhD thesis, Valencia (2002); (b) R. Lescouëzec, F. Lloret, M. Julve, J. Vaissermann, M. Verdaguer. *Inorg. Chem.*, **41**, 5943 (2002).
[11] S. Wang, X. Ding, J. Zuo, X. You, W. Huang. *Coord. Chem. Rev.*, **255**, 1713 (2011).
[12] P. Ferko, S.M. Holmes. *Curr. Inorg. Chem.*, **3**, 172 (2013).
[13] K. Ridier, A. Mondal, C. Boilleau, O. Cador, B. Gillon, G. Chaboussant, B. Le Guennic, K. Costuas, R. Lescouëzec. *Angew. Chem. Int. Ed.*, **55**, 3963 (2016).
[14] D. Aguila, Y. Prado, E. Koumousis, C. Mathonière, R. Clérac. *Chem. Soc. Rev.*, **45**, 203 (2016).
[15] (a) T. Liu, Y.-J. Zhang, S. Kanegawa, O. Sato. *J. Am. Chem. Soc.*, **132**, 8250 (2010); (b) J. Yang, L. Zhou, J. Cheng, Z. Hu, C. Kuo, C.-W. Pao, L. Jang, J.-F. Lee, J. Dai, S. Zhang, S. Feng, P. Kong, Z. Yuan, J. Yuan, Y. Uwatoko, T. Liu, C. Jin, Y. Long. *Inorg. Chem.*, **54**, 6433 (2015); (c) D.-P. Dong, T. Liu, S. Kanegawa, S. Kang, O. Sato, C. He, C.-Y. Duan. *Angew. Chem., Int. Ed.*, **51**, 5119 (2012); (d) N. Hoshino, F. Iijima, G.N. Newton, N. Yoshida, T. Shiga, H. Nojiri, A. Nakao, R. Kumai, Y. Murakami, H. Oshio. *Nat. Chem.*, **4**, 921 (2012).
[16] J.-R. Jiménez, A. Mondal, L.-M. Chamoreau, P. Fertey, F. Tuna, M. Julve, A. Bousseksou, R. Lescouëzec, L. Lisnard. *Dalton Trans.*, **45**, 17610 (2016).
[17] (a) J.-R. Jiménez, M. Tricoire, D. Garnier, L.-M. Chamoreau, J. Van Bardeleden, Y. Journaux, Y. Li, R. Lescouëzec. *Dalton Trans.*, **46** (2017); (b) D. Garnier, J.-R. Jiménez, Y. Li, J. von Bardeleben, Y. Journaux, T. Augenstein, E. Moos, M. Gamer, F. Breher, R. Lescouëzec. *Chem. Sci.*, **7**, 4825 (2016).
[18] Trofimenko. *Scorpionates, The coordination chemistry of polypyrazolylborate ligands*, Imperial College Press, London (1999).
[19] S. Trofimenko. *J. Am. Chem. Soc.*, **89**, 3170 (1967).
[20] D. Li, S. Parkin, D. Wang, G.T. Yee, R. Clérac, W. Wernsdorfer, S.M. Holmes. *J. Am. Chem. Soc.*, **126**, 4214 (2006).
[21] S. De. PhD thesis, UPMC, Paris (2016).
[22] I. Bertini, C. Luchinat, G. Parigi. Solution NMR of paramagnetic molecules. In *Curr. Methods in Inorganic Chemistry*, Elsevier, Amsterdam (2001).
[23] R.K. Harris, E.D. Becker, S.M. Cabral de Menezes, R. Goodfellow, P. Granger. *Pure Appl. Chem.*, **73**, 1795 (2001).
[24] F.H. Koehler, O. Storcheva. *Inorg. Chem.*, **54**, 6801 (2015).
[25] D. Garnier. PhD thesis, KIT (Karlsruhe) – UPMC (Paris), ISBN 978-3-8325-4091-3 (2015).
[26] M. Nihei, M. Ui, N. Hoshino, H. Oshio. *Inorg. Chem.*, **47**, 6106 (2008).
[27] (a) J.F. Endicott, Y.J. Chen. *Coord. Chem. Rev.*, **257**, 1676 (2013); (b) J.-P. Launay. *Chem. Soc. Rev.*, **30**, 386 (2001).
[28] (a) E. Pardo, M. Verdaguer, P. Herson, H. Roussellière, J. Cano, M. Julve, F. Lloret, R. Lescouëzec. *Inorg. Chem.*, **50**, 6250 (2011); (b) D. Li, S. Parkin, G. Wang, G.T. Yee, A.V. Prosvirin, S.M. Holmes. *Inorg. Chem.*, **44**, 4903 (2005); (c) D. Li, S. Parkin, R. Clérac, S.M. Holmes. *Inorg. Chem.*, **45**, 7569 (2006).
[29] O. Kahn, *Molecular Magnetism*, Wiley VCH (1993).
[30] N.F. Chilton, R.P. Anderson, L.D. Turner, A. Soncini, K.S. Murray. *J. Comput. Chem.*, **34**, 1164 (2013).
[31] D. Wu, Y. Zhang, W. Huang, O. Sato. *Dalton Trans.*, **23**, 5500 (2010).